



Graduate Theses, Dissertations, and Problem Reports

2000

Synthesis and characterization of metal oxide nanoparticles

Heidi Jo Magnone
West Virginia University

Follow this and additional works at: <https://researchrepository.wvu.edu/etd>

Recommended Citation

Magnone, Heidi Jo, "Synthesis and characterization of metal oxide nanoparticles" (2000). *Graduate Theses, Dissertations, and Problem Reports*. 1129.
<https://researchrepository.wvu.edu/etd/1129>

This Thesis is protected by copyright and/or related rights. It has been brought to you by the The Research Repository @ WVU with permission from the rights-holder(s). You are free to use this Thesis in any way that is permitted by the copyright and related rights legislation that applies to your use. For other uses you must obtain permission from the rights-holder(s) directly, unless additional rights are indicated by a Creative Commons license in the record and/ or on the work itself. This Thesis has been accepted for inclusion in WVU Graduate Theses, Dissertations, and Problem Reports collection by an authorized administrator of The Research Repository @ WVU. For more information, please contact researchrepository@mail.wvu.edu.

SYNTHESIS AND CHARACTERIZATION OF METAL OXIDE NANOPARTICLES

Heidi J. Magnone

Thesis submitted to the College of Arts and Sciences at West Virginia University in
partial fulfillment of the requirements for the degree of

Master of Science
In
Physics

Dr. Mohindar S. Seehra, Chair
Dr. John E. Littleton
Dr. Wathiq Abdul-Razzaq

Department of Physics

Morgantown, West Virginia
2000

Keywords: Nanoparticle, Synthesis, Sol-Gel, Electrochemical, Copper Oxide, Cobalt
Oxide, Manganese Oxide, Nickel Oxide, CuO, Co₃O₄, Mn₅O₈, NiO

ABSTRACT

SYNTHESIS AND CHARACTERIZATION OF METAL OXIDE NANOPARTICLES

HEIDI MAGNONE

Nanoparticles of CuO, Co₃O₄ and Mn₅O₈ were prepared via sol-gel chemical routes. Thermal treatments of the gels were used to obtain particles of different sizes, as determined by the widths of the Bragg lines in x-ray diffraction. To prepare CuO nanoparticles, a Cu(OH)₂ gel was first produced by reacting copper nitrate with sodium hydroxide, followed by annealing the gel at temperatures between 160°C to 1,000°C to produce particles in the 6 to 36 nm range. Nanoparticles of Co₃O₄ in the size range of 9 to 45 nm were prepared in an analogous manner by reacting cobalt nitrate and sodium hydroxide. Similar procedures to produce nanoparticles of MnO resulted only in the synthesis of Mn₃O₄. Annealing Mn₃O₄ at 400°C for three hours produced nanoscale Mn₅O₈ (14nm), a difficult-to-prepare oxide. Using an electrochemical route, 30nm particles of NiO were also synthesized. Thermogravimetric measurements were used to identify the thermally-induced phase transformations and x-ray diffraction was used to identify the phases and determine the average particle sizes of the phases.

ACKNOWLEDGEMENTS

I would like to express my sincere appreciation to my research advisor Dr. Mohindar S. Seehra for his patience, guidance and instruction, and for the valuable research opportunities that he provided for me. I also thank Alex Punnoose for his constant encouragement and helpful comments. The financial support provided by the U.S. Department of Energy (Contract #DE-FC26-99FT40540) to this research project is also acknowledged.

TABLE OF CONTENTS

| | Page |
|--|------|
| Abstract | ii |
| Acknowledgments | iii |
| Table of Contents | iv |
| List of Figures | vi |
| I. Introduction | 1 |
| II. Fundamentals of Sol-Gel Processing | 2 |
| 2.1 Reaction of Chemical Precursors | 4 |
| 2.2 Gelation | 10 |
| 2.3 Drying | 13 |
| 2.4 Annealing | 14 |
| III. Sol-Gel Preparation of CuO, Co ₃ O ₄ and Mn ₅ O ₈ Nanoparticles | 17 |
| 3.1 CuO Nanoparticles | 17 |
| a. Literature Review | 17 |
| b. Synthesis | 18 |
| c. Characterization | 19 |
| 3.2 Co ₃ O ₄ Nanoparticles | 22 |
| a. Literature Review | 22 |
| b. Synthesis | 23 |
| c. Characterization | 23 |
| 3.1 Mn ₅ O ₈ Nanoparticles | 26 |
| a. Literature Review | 26 |
| b. Synthesis | 26 |
| c. Characterization | 27 |
| IV. Fundamentals of Electrochemical Synthesis | 30 |

| | | |
|-----|--|----|
| V. | Electrochemical Preparation of NiO Nanoparticles | 32 |
| | a. Literature Review | 32 |
| | b. Synthesis | 32 |
| | c. Characterization | 32 |
| VI. | Results and Conclusions | 33 |
| | References | 35 |
| | Vita | 38 |

LIST OF FIGURES

| Figure | | Page |
|--------|--|------|
| 2.1 | The Sol-Gel Route | 3 |
| 2.2 | Critical Radius of Nucleation | 5 |
| 2.3 | Electrostatic Double-Layer Repulsion | 8 |
| 2.4 | Potential Energy Between Two Particles | 10 |
| 2.5 | Lateral vs. Linear Linkage of Particles | 11 |
| 2.6 | Neck Formation | 12 |
| 3.1 | X-Ray Diffraction Pattern for CuO | 20 |
| 3.2 | CuO Particle Size vs. Annealing Temperature | 21 |
| 3.3 | Thermogravimetric Analysis of Cu(OH) ₂ | 22 |
| 3.4 | X-Ray Diffraction Pattern for Co ₃ O ₄ | 24 |
| 3.5 | Co ₃ O ₄ Particle Size vs. Annealing Temperature | 24 |
| 3.6 | Thermogravimetric Analysis of Co(OH) ₂ | 26 |
| 3.7 | X-Ray Diffraction Pattern for Mn ₅ O ₈ | 27 |
| 3.8 | Thermogravimetric Analysis of Mn ₃ O ₄ | 29 |
| 4.1 | Electrochemical Production of NiO Nanoparticles | 31 |
| 4.2 | X-Ray Diffraction Pattern for NiO | 33 |

I. INTRODUCTION

Particles of size range 1-100 nm are considered nanoscale.¹ These nanoparticles, and structures and devices comprised of them, display unique mechanical, optical, electrical, and magnetic properties that differ radically from the corresponding bulk material.¹ Applications of nanostructured materials include catalysts, electrolyte membranes, films, and fibers. Current intense research in nanoparticles has created a great demand for their efficient production.

Nanoparticles can be produced through either chemical or physical means. They can be made physically by ball milling, a process in which coarse particles are ground to nanoscale particles. Disadvantages of ball-milling include the high mechanical energy needed (resulting in strain in the particles) and contamination by the material of which the ball mill is made. In chemical methods, by-products form during reactions but they can generally be removed. Chemical techniques provide the power to mix at the molecular level, allowing for the production of highly homogeneous materials.

Nanoparticles can be synthesized chemically through sol-gel processing, electrochemical methods,² hydrothermal techniques,³ and chemical vapor deposition.⁴ This work explores sol-gel and electrochemical synthesis. CuO, Co₃O₄ and Mn₅O₈ nanoparticles as small as 6.1, 9.4, and 14.0 nm respectively were synthesized through sol-gel chemistry using metallic salt precursors. 30nm-NiO particles were obtained through electrochemistry.

II. FUNDAMENTALS OF SOL-GEL PROCESSING

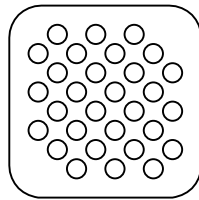
Sol-gel processing is convenient for its simple procedures, requiring little more than standard solution chemistry. The initial aim in the sol-gel technique is to produce a sol, which is a suspension of solid colloidal particles in a liquid. The colloidal particles may or may not have the chemical composition of the desired end-product. The particles, through van der Waals attraction, eventually connect to form a gel, a 3-dimensional solid network having high porosity and high specific surface area. The gel can simply be dried and ground if a nanoscale powder is the aim. The wet sol may be deposited onto a substrate and then allowed to gel if a thin film is desired. The gel may be heated to induce chemical phase changes, or to densify a thin film or ceramic structure.

Sol-gel chemistry is used mainly to produce metal oxides, but production of carbides, nitrides, and sulfides is also possible through this route⁵. Metal oxides can be synthesized directly in the initial chemical reaction, or a metal hydroxide may form which can be heated to yield the oxide.

Metallic salts (M_mX_n), alkoxides ($M(OR)_n$), and, less commonly, organometallics (MR) are used as chemical precursors (M is a metal, X is an anion, R is an alkyl (carbon) group) in sol-gel processing.⁵ In this work, metal salt precursors are used to produce CuO, Co_3O_4 and Mn_5O_8 nanoparticles. Addition of sodium hydroxide to a metal nitrate solution yields a metal hydrous oxide sol, which can be annealed to obtain various phases of oxide. Many metal oxide nanoparticles have been made from metal-salt precursors, including CuO,⁶ Co_3O_4 ,⁷ NiO,⁸ Fe_2O_3 ,⁹ Fe_3O_4 ,¹⁰ TiO_2 ,¹¹ ZrO_2 ¹² and ZnO.¹³

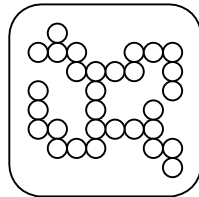
The four steps in sol-gel processing are: (1.) Reaction of the appropriate chemical precursors to form colloidal particles; (2.) Aggregation of particles to form a gel; (3.) Drying of the gel; (4.) Heating to induce phase transformations and/or densification (see figure 2.1).

1. Reaction of Precursors to Form Sol



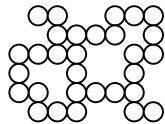
Colloidal Solid
Particles in
Liquid

2. Gelation



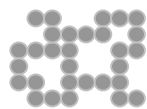
3-Dimensional
Network in
Liquid

3. Drying



Removal of
Liquid to Obtain
a Xerogel

4. Annealing



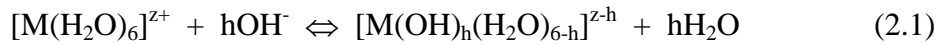
Heating Induces
Phase Transformations

Figure 2.1. The Sol-Gel Route

2.1 REACTION OF CHEMICAL PRECURSORS

For metallic salt precursors, water is an appropriate choice of solvent and it is used exclusively in this work. Various nonaqueous solvent mixtures are also commonly used, depending on the precursors chosen.⁵

When a metal salt, MX, is dissolved in water, a hydrated metal cation, $M(H_2O)_6^{z+}$, is formed where z is the oxidation number.¹⁴ Addition of a base gives a hydrolyzed metal complex via the following reaction:⁵



When h is equal to z, the charge of the metal complex is neutralized and the solid hydroxide, $M(OH)_z(H_2O)_{6-z}$, precipitates. Along with the neutral hydroxide, charged complexes (positive at high pH and negative at low pH) are also expected to form but they are water-soluble and so will not precipitate.

Nucleation and Growth of Particles. Metal hydroxide molecules in the water are drawn to one another through van der Waals forces. With the help of random thermal motion, they come into contact with one another, then bond chemically to form crystals.

The total free energy to form a solid particle of a particular type of material is dependent on the particle size. Assuming for simplicity a spherical particle of radius r, the free energy is⁵

$$\Delta G_r = \Delta G_s + \Delta G_i \quad (2.2)$$

where ΔG_s is the contribution to the free energy due to the surface, and ΔG_i is the contribution due to the phase transformation inside the particle. ΔG_s and ΔG_i can be expressed as⁵

$$\Delta G_s = 4\pi r^2 \Delta\gamma > 0 \quad (2.3)$$

$$\Delta G_i = \left(\frac{4}{3}\right) \pi r^3 \Delta G_v < 0 \quad (2.4)$$

where $\Delta\gamma$ is the surface energy and ΔG_v is the difference in the free energy per unit volume of the final phase and initial phase. For very small values of r , the positive surface contribution is dominant, making ΔG_r positive. Because the change in free energy ΔG_r must be negative for any process to occur spontaneously, the existence of very small particles (resulting in positive ΔG_r) is thermodynamically unfavorable.

There exists a critical radius, r_c , such that particles of smaller radius dissolve and those of larger radius grow (see figure 2.2). Despite their thermodynamic instability,

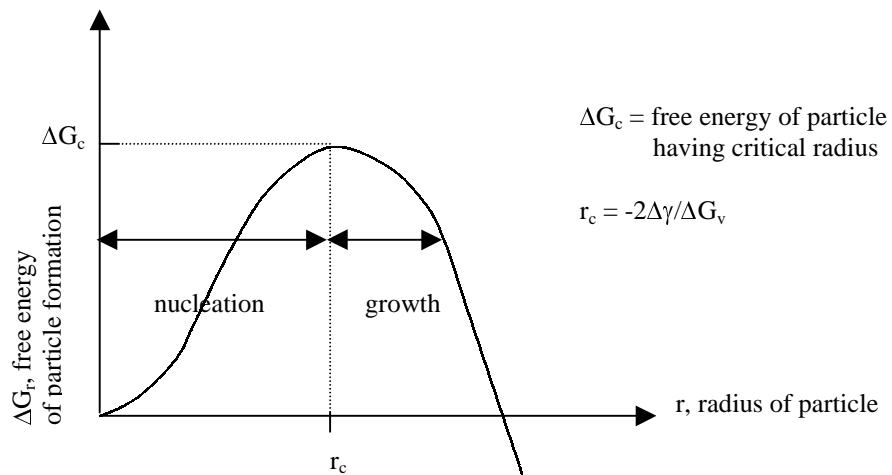


Figure 2.2. Critical Radius of Nucleation

small particles must form, of course, before they can grow to larger, more stable ones. The continual random thermal motion of solute molecules will cause them to come into contact with one another to form aggregates of subcritical radii.¹⁵ Most of these aggregates, termed embryos, will dissolve but Brownian motion ensures a finite probability that some will survive long enough to collide with other embryos to form particles of radius $r > r_c$.¹⁵ These particles, called nuclei, are about 1nm and will grow by deposition of solute molecules onto their surfaces.⁵ Increase in particle size by nucleus-nucleus coagulation becomes increasingly unlikely as nuclei grow—mutual electrostatic repulsion exists between growing nuclei due to surface charges that develop.

The formation of a sol, a suspension of solid colloidal particles in a liquid, is paramount in sol-gel processing. Colloidal particles are of size range 2nm to 0.2 μ m, which corresponds to about 10^3 to 10^9 atoms.⁵ Smaller particles have a tendency to redissolve after they form, while larger particles fall out of suspension (hindering gelation) as gravitational forces overcome dispersive forces.

The smallest particles are expected to form from either very high or very low concentrations of reagents. At intermediate concentrations, larger particles form. In dilute solutions, the solute molecules are far apart from one another and from growing nuclei, therefore nuclei grow slowly. Plenty of time is available for new nuclei to form before older nuclei seize all of the available solute molecules for their own growth. This limits the final size achieved by older nuclei. After all molecules have been deposited on particles, growth is halted, leaving older nuclei larger and younger nuclei smaller. The result is a polydisperse sample of small average particle size.

At high concentrations, the solute molecules are close together so that many nuclei form quickly and almost simultaneously. Most of the solute is initially used up in forming nuclei. Few molecules are left over to support further growth by deposition onto the surfaces of nuclei. A monodisperse sample of small particles is the outcome.

Stability of Particles: The Electrical Double Layer. Metal hydroxide particles, and also metal oxide particles since they generally have surface hydroxyl groups, carry a surface charge dependent upon the specific compound formed and the pH. The surface charge is acquired by adsorption of H⁺ or OH⁻ ions onto the particle surface. In acidic solution, particles gain a positive charge.¹⁶



Under basic conditions, particles carry negative charge.¹⁶



The pH below which the particles are positively charged, and above which are negatively charged, is called the zero point charge, or z.p.c.. The z.p.c., at which the particles are electrically neutral, is a characteristic of the type of material. For hydroxide and oxide compounds, z.p.c.'s vary greatly, ranging anywhere from a pH of 1 to 12.^{17, 18}

Ions in solution having a charge opposite to that of the particles are termed counterions. In these experiments, metal nitrate precursors are used with an excess of sodium hydroxide so that the particles carry a negative charge and the sodium cations

take on the role of the counterions. The counterions are drawn toward the particle surface and layer themselves around it. The surface charges with their blanket of counterions comprise what is termed the electrical double layer.

From a distance, the electrical double layer makes particles appear to one another electrically neutral. But at close range, where the double layers may interpenetrate, particles experience mutual electrostatic repulsion. This electrostatic repulsion manifest

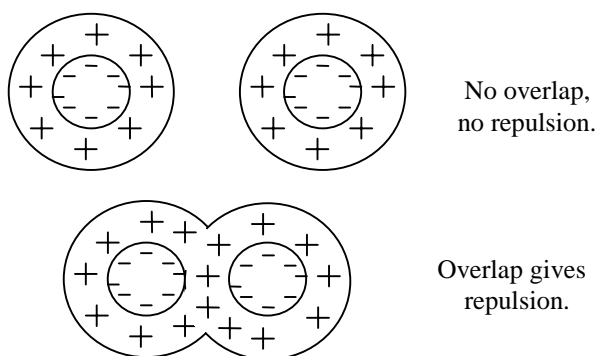


Figure 2.3. Electrostatic Double-Layer Repulsion

at close contact prevents particle coagulation. Colloidal dispersions stabilized by electrical double layers are termed “electrostatic sols,” in contrast to “steric sols” which are stabilized by surfactants of large, electrically neutral organic molecules which create a steric, or physical, barrier between particles. (The NiO particles discussed in sections IV. and V. were stabilized through steric means.) Electrostatic stability is lost at the z.p.c. where no electrical double later exists.

In the presence of an applied electric field, positively charged particles move with the field while negatively charged particles move antiparallel to it. A particle moving in a field will carry along with it many of its counterions and some surrounding fluid.

Therefore, a shear surface exists between the liquid moving with the particles and the stationary liquid. The electric potential at the shear surface is called the zeta potential, ζ . The isoelectric point, or i.e.p., is the pH for which $\zeta=0$. At the i.e.p., the electrical mobility is zero, while at the z.p.c. surface charge is zero. Because electrophoretic mobility is often convenient to measure, i.e.p.'s are often reported rather than z.p.c.'s. Values for the i.e.p. and the z.p.c. are close enough to be used interchangeably in practice. They are regarded as equivalent in this work.

The van der Waals attraction between particles (which diminishes as $1/d^6$, d is the distance between particles) tends to bring them together and promotes coagulation, while the electrical double layer (diminishes as $1/d^2$) tends to keep particles independent. The interplay of van der Waals attraction and electrostatic repulsion between two particles is represented by the curve of figure 2.4.¹⁶ The curve for particle distance less than zero is due to repulsion from electron cloud interpenetration. The repulsive barrier prevents particles from achieving close contact and falling into the primary minimum where coagulation is inescapable and specific surface area is irreversibly reduced. When the barrier height is diminished below kT (the thermal kinetic energy of the particle where k is the Boltzmann constant and T is the absolute temperature), as occurs near the z.p.c., particles coagulate. With a barrier of sufficient height, particles will generally eventually settle into the secondary minimum, a process called flocculation. A floc is an aggregate of particles that are connected to one another, yet remain individual entities so that very little reduction in surface area results. Flocculation is often reversible—a little agitation can break up flocs and redisperse the particles. The formation of flocs marks the beginning of gelation.

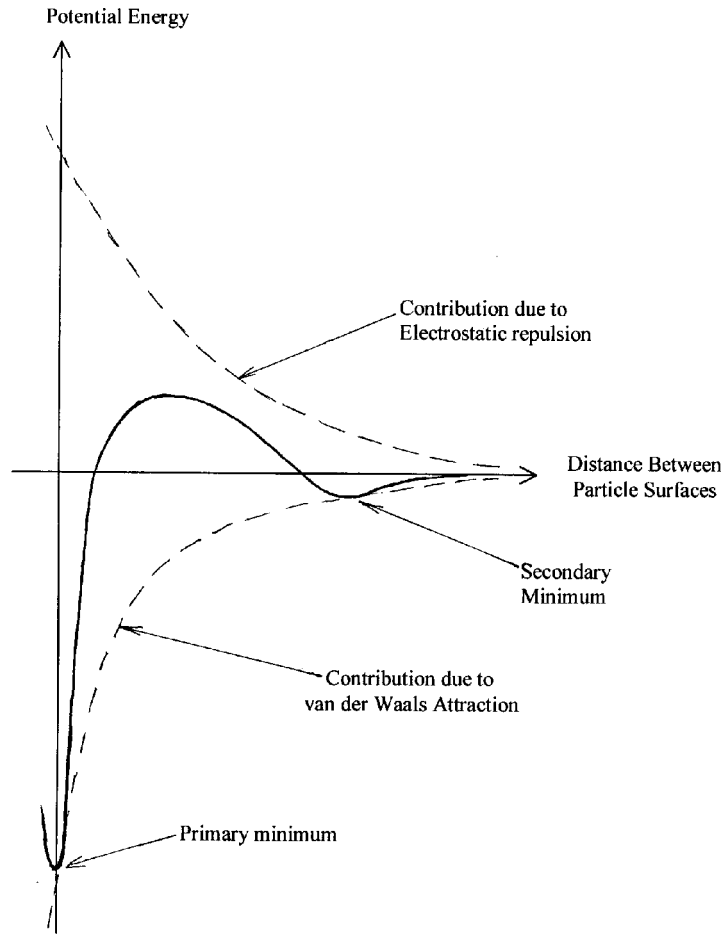


Figure 2.4. Potential Energy Between Two Particles

2.2 GELATION

Metal hydroxide suspensions are rarely stable indefinitely. Due to their Brownian motion, particles will make close enough approach to fall into the secondary minimum of figure 2.4 so that flocs are formed. Eventually, floc joins to floc, forming a three-dimensional network throughout the liquid. This process, called gelation, is noted by an increase in viscosity of the solid-liquid mix. Gelation allows for the formation of porous, open structures because of the way in which particles preferentially connect.

When two particles connect, the way in which the electrical double layer configures itself creates greater electrostatic repulsion for lateral linkage than for linear linkage of a third particle.⁵ According to DLVO theory (named after its developers, Derjaguin, Landau, Verwey, and Overbeek), the repulsion for lateral approach is greater than for linear approach by a factor of the order of the square root of 2.⁵ Therefore linear chains of particles develop with occasional lateral bridges connecting them, resulting in open structures of high surface area. Near the z.p.c., where the electrical double layer repulsion is slight, repulsion for lateral approach is so diminished that dense aggregates form and coagulation is imminent (see figure 2.5).

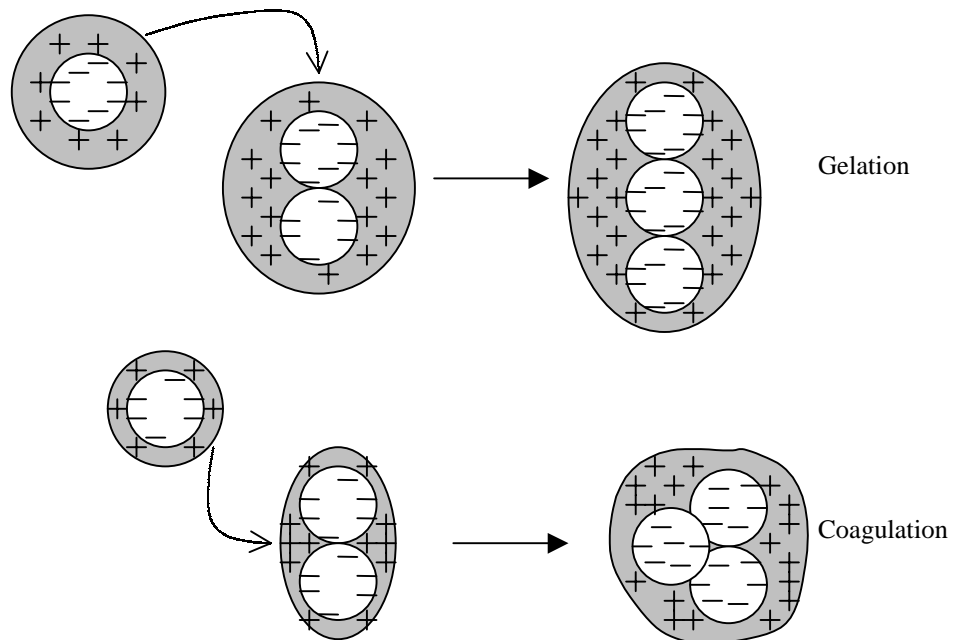


Figure 2.5. Lateral vs. Linear Linkage of Particles

Coarsening of The Gel Structure. The higher the specific surface area of the gel, the less thermodynamically stable it is. Therefore any mechanism available to drive

down the surface area will operate. For a solid gel network in a liquid, coarsening, also referred to as ripening, causes surface area reduction.¹⁶

Coarsening is a smoothing of the surfaces of gel pores through dissolution and reprecipitation. The solubility of the surface of a solid is given by¹⁶

$$s = s_0 \exp(2\gamma V_m / R_g T r) \quad (2.7)$$

where s_0 is the solubility of the particular solid material, γ is the energy of the solid-liquid interface, V_m is the molar volume of the solid, R_g is the ideal gas constant, T is the absolute temperature, and r is the radius of curvature of the solid. A particle has a positive radius of curvature, while crevices between particles have negative radii, so that solubility is higher on particle surfaces than in crevices. Therefore, there is a tendency for material to dissolve from particle surfaces and then redeposit into crevices. This causes necks to form between particles, reducing the total surface area and stiffening the gel network (see figure 2.6).

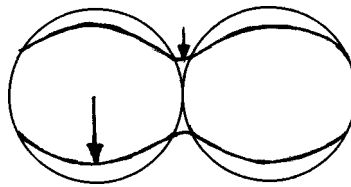


Figure 2.6. Formation of Necks

Washing the gel with water removes water-soluble impurities, but carries away counterions that stabilize particles via the electrical double layer. However, the necks,

which unfortunately reduce surface area, stabilize the gel by providing the open network with the mechanical strength needed to resist pore collapse.

2.3 DRYING

Shrinkage. The capillary forces that develop during the drying stage can cause gels to shrink by a factor of 5 to 10.¹⁶ The energy associated with the solid-vapor interface is greater than that of the solid-liquid interface. Therefore, as liquid evaporates from the gel's outer surface, the gel contracts in an effort to avoid exposure of the solid phase to the air. As the gel shrinks, all pores tend to remain saturated with liquid, so that the decrease in gel volume matches the volume of liquid evaporated.¹⁶

Shrinkage under capillary stresses is possible because the network of the wet gel is very flimsy, with its long strings of particles and huge pores. The strings of particles can bend and additional bridges between them can be built. This restructuring of the network results in denser packing of particles, pore size reduction, and some decrease in surface area (although the surface area of the dry gel is still extremely high, from 100 to 1,000 m²/g).⁵ At some point, the particles crowd, making additional rearrangements less likely. The network stiffens, so that the gel becomes strong enough to resist capillary stresses and shrinkage ceases. When the gel can shrink no more, the solid-vapor interface recedes below the gel's outer surface and the pores become unsaturated, containing both liquid and vapor.¹⁶ The dried gel is a solid unit in its own right, with elastic, shear, and bulk moduli that are not, in general, equivalent to that of the bulk material.

Cracking. The liquid is in tension as it is drawn from the gel's interior to its outer surface. Compressive stresses in the solid act to balance the tension and the gel shrinks.

The decrease in pore size as the gel shrinks lowers the permeability, making it increasingly difficult to draw out liquid.¹⁶ Pressure gradients develop such that the tension in the liquid is greater in the exterior regions than in the interior. The surface contracts faster than the inside of the gel, inducing cracking.¹⁶

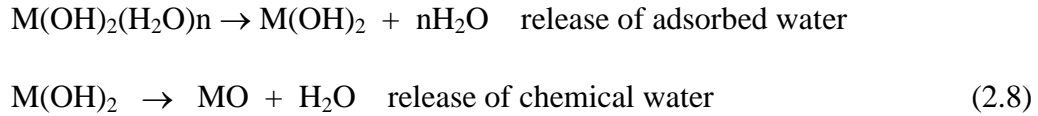
Permeability is usually large enough in ordinary ceramics to reduce pressure gradients so that cracking is eliminated, but with gels cracking is difficult to avoid. When the gel is to be used for some application, such as a film or coating, preventing cracking is crucial. Supercritical drying, drying at a critical temperature and pressure eliminating capillary stresses, produces gels which do not shrink or crack.¹⁶ Gels from supercritical drying are called aerogels, while gels obtained from normal evaporation are called xerogels. Because for these experiments the desired end-products are metal oxide powders, cracking is not a concern and only xerogels are produced.

2.4 ANNEALING

Phase Transformations. As the temperature is elevated, a gel passes through various phase transitions until at some high temperature, depending on the nature of the gel but often around 1,000 °C, the most thermodynamically stable state is achieved.⁵ What transition phases appear at specific temperatures is very sensitive to the initial conditions under which the gel was made, such as temperature, pH, and concentrations of reactants. Rare, metastable phases, sometimes difficult to reproduce, have been documented.⁵

Low Temperature Annealing of Metal Hydroxides. As the temperature of a metal hydroxide gel is raised above ambient, the first change noted is loss of water.

Adsorbed, or *residual*, water is released first, and then *chemical*, or *structural*, water. For example, for +2 metal cations,



Release of residual and structural water results in a drop in mass as evidenced by TGA (thermogravimetric analysis). Mass loss of a gel due to water expulsion often occurs at temperatures in the range of 100-300°C.⁵ The ratio of adsorbed to structural water usually depends on the chemical recipe used in the gel preparation.⁵

Throughout the expulsion of structural water, and the phase transformation due to release of chemical water, the crystallographic structure remains intact. The gel shrinks as it loses mass, but the phase transformation is *topotactic*, meaning that a monocrystal of hydroxide remains, roughly, a monocrystal as it transforms to a metal oxide.⁵ At the low temperatures at which water departs, oxygen anions do not have enough thermal energy to move from their lattice positions, making reorganization of oxygen impossible. Very little reduction in surface area occurs during topotactic transformations.

Pore Evolution. Below a critical temperature, which depends on the particular gel, but is generally between 500 and 1,000 °C, the size of the pores remains fairly stable.⁵ In this temperature range, material from particle surfaces is transported through surface atomic diffusion to the necks. The filling in of the necks tends to smooth out pore surfaces, which reduces total surface area, but does not result in changes in pore size.

Changing pore size requires the movement of atoms within the lattice, which occurs at higher temperatures.

The gradual removal of the porosity through lattice diffusion is a process called *sintering*, or *densification*, which results in a large decrease in specific surface area due to changes in pore size and in the number of pores. The specific surface area may decrease by a factor of 10 during the sintering process.⁵ There is the tendency at high temperature, often around 1,000°C, for lattice atoms to diffuse from larger pores to smaller ones.⁵ Atoms in the vicinity of some point on the surface of a spherical pore are under a tensile mechanical stress, σ ,⁵

$$\sigma = -2\gamma/r \quad (2.9)$$

where γ is the pore surface tension and r is the pore radius. A small radius corresponds to a large stress, so that material is transported through diffusion from larger pores to smaller ones, closing smaller pores and causing larger ones to grow, in order to relieve stress in the system. The result is a decrease in the total number of pores, an increase in average pore size, decrease in specific surface area, and decrease in crystallite size.

III. SOL-GEL PREPARATION OF CuO, Co₃O₄ AND Mn₅O₈ NANOPARTICLES

3.1 CuO NANOPARTICLES

a. Literature Review

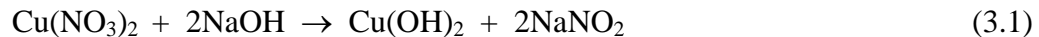
CuO nanoparticles have been synthesized from copper (II) acetate using sonochemical techniques¹⁹ and spin-coating methods.²⁰ They have also been produced electrochemically through corrosion of a copper metal anode.²¹ In this work, CuO nanoparticles were synthesized through a sol-gel chemical route used previously to produce NiO nanoparticles.⁸ Results of magnetic studies performed on these CuO samples have been submitted for publication to *Physical Review B*.

In our experiment, a 0.1M Cu(NO₃)₂, copper nitrate, aqueous solution was reacted at room temperature with a 1M NaOH, sodium hydroxide, aqueous solution to obtain a Cu(OH)₂, copper (II) hydroxide, suspension. The Cu(OH)₂ was filtered, dried, powdered and annealed at temperatures between 160°C and 1000°C to get CuO nanoparticles of size range 6.1 to 36nm. In reviewing the literature it was found that Lee, Her, and Matijevic had also produced CuO particles of a similar size range from reaction of Cu(NO₃)₂ and NaOH, but their procedure was different.⁶ They performed a reaction of 0.1M aqueous Cu(NO₃)₂ and NaOH, concentrations in a range of 0.1 to 0.21M, at various temperatures. Their resulting *Cu(OH)₂ aqueous suspension* was aged for a period of time at the reaction temperature to induce conversion to a *CuO aqueous suspension*. Then the CuO particles were separated by centrifugation and dried to obtain a powder. Their

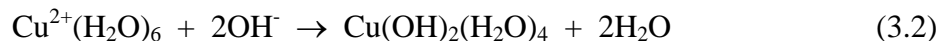
samples were prepared at reaction temperatures of 20, 40, 50, and 90°C and were aged for 5 days, 30min, 15min, and 10min respectively. In another study by Kratochvil and Matijevic, a Cu(OH)₂ suspension was dried and powdered, then annealed at 500C to get CuO particles which appear from their SEM pictures to be in the micrometer size range.²² However, the aim in both of their studies was actually to produce small particles of uniform size and shape rather than to achieve the smallest possible particle size. The exact procedure outlined in this thesis for producing CuO particles in the lower-nanometer range was not found to be documented anywhere in the literature.

b. Synthesis

Preparation of Cu(OH)₂ Gel. 125mL of a 1M NaOH aqueous solution was added all at once to 200mL of a 0.1M Cu(NO₃)₂ aqueous solution (pH = 13) to obtain a Cu(OH)₂ blue suspension.



The above reaction occurs through deprotonation of the hydrated Cu²⁺ cation:¹⁴



In a pH of 10 and above, the complexes Cu(OH)₃⁻ and Cu(OH)₄²⁻ are also expected to form,¹⁴ but they are water-soluble and so will not precipitate. The pH of 13 was far from the i.e.p. of Cu(OH)₂, which is pH=7.6,¹⁷ to ensure electrostatic stabilization by charged particles.

Gelation was evident as the $\text{Cu}(\text{OH})_2$ -plus-water mixture appeared to become more viscous. The gel was separated by filtration, washed with water and filtered. It was then dried in an oven at 50°C overnight, over which time it shrunk to approximately one-fifth its original size. The product dried to a hard, low-density, blue solid unit. The gel was ground to a powder.

Transformation of $\text{Cu}(\text{OH})_2$ to CuO . The copper hydroxide powder was annealed at various temperatures to obtain CuO nanoparticles.



The existence of pure CuO and the size of the particles were determined by x-ray diffraction (XRD) using a Rigaku D/Max diffractometer.

c. Characterization

The average particle sizes of the CuO samples were determined from the x-ray diffraction patterns. Broad peaks correspond to small particles, while large particles are indicated by narrow peaks. The average crystallite dimension, L_{hkl} , where hkl indicates the Miller indices of the Bragg peak to be analyzed, can be calculated from the Scherrer formula,²³

$$L_{\text{hkl}} = K\lambda/\beta\cos\theta \quad (3.4)$$

where $K = 0.9$, $\lambda = 0.1542\text{nm}$ is the wavelength of the x-rays, β is the extra width in radians, and θ is the Bragg angle of the peak. β includes a correction that takes into account the instrumental broadening. It is calculated from

$$\beta^2 = B^2 - b^2 \quad (3.5)$$

where B is the full width at half maximum of the chosen Bragg peak for the sample, and b is the width of a peak near θ for a standard sample, which for these studies was a SiO_2 crystal.

CuO nanoparticles of sizes 6.1, 7.8, 8.8, 11.6, 16.4, 25.7, 34.5 and 36.0 nm were obtained from annealing temperatures of 160, 200, 250, 300, 400, 600, 800 and 1,000°C respectively. XRD detected no other phases (see figure 3.1), which is significant because

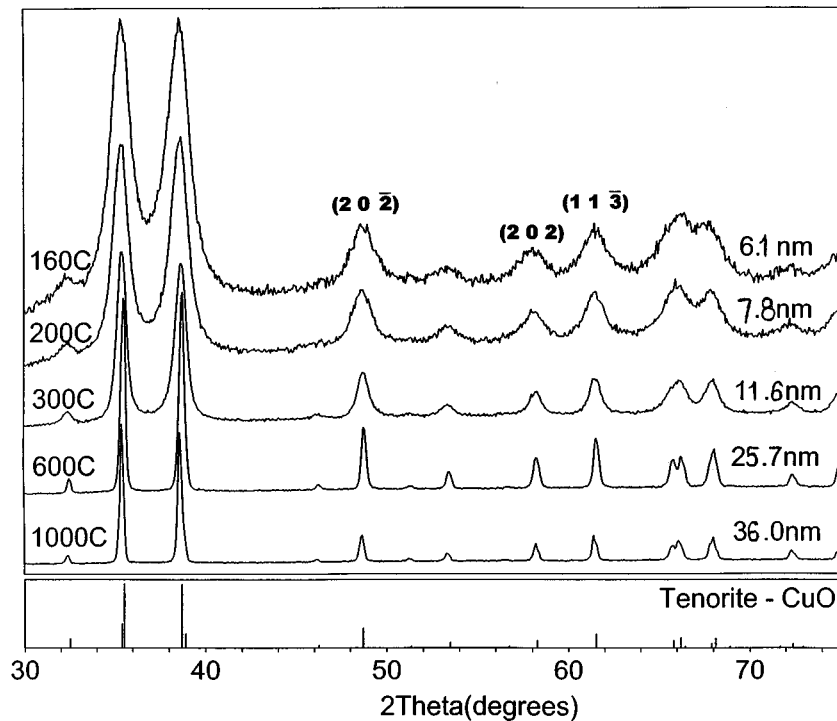


Figure 3.1. X-Ray Diffraction Pattern for CuO

Palkar et al have reported that CuO particles smaller than 25nm are unstable, transforming to Cu₂O.²⁴ CuO particle size was found to increase with increasing annealing temperature (see figure 3.2). The lowest temperature at which the Cu(OH)₂ gel converts to CuO was found to be about 160°C, and at this temperature the smallest particles of 6.1nm formed. TGA (thermogravimetric analysis) confirmed this conversion temperature.

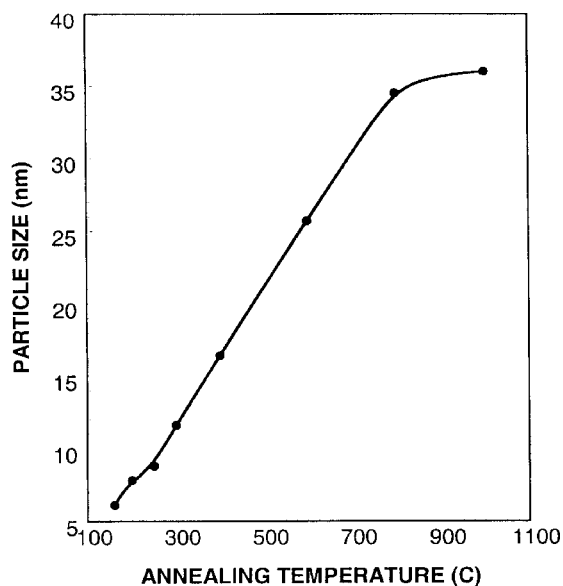


Figure 3.2. CuO Particle Size vs. Annealing Temperature

TGA revealed that 0.77mg of adsorbed water was released from a 26.6mg sample of Cu(OH)₂ gel as the temperature rose from 25 °C to about 130 °C, showing that residual water comprised 2.3% of the original room-temperature gel (see figure 3.3).

Over a temperature range of about 130 to 190°C, 4.81mg of structural water were released as Cu(OH)₂ converted to CuO. This shows that the Cu(OH)₂ lost 4.81/25.83 =

18.6% of its weight due to chemical water loss, in close agreement with the theoretical value of 18.5%.

$$\begin{aligned} & (\text{Molecular weight of water/molecular weight of Cu(OH)}_2) * 100\% \\ & = (18.02/97.57) * 100\% = 18.5\% \end{aligned} \quad (3.6)$$

The temperature range of conversion to CuO is in excellent agreement with the range of 140 - 180°C found by Ramamurthy and Secco.²⁵

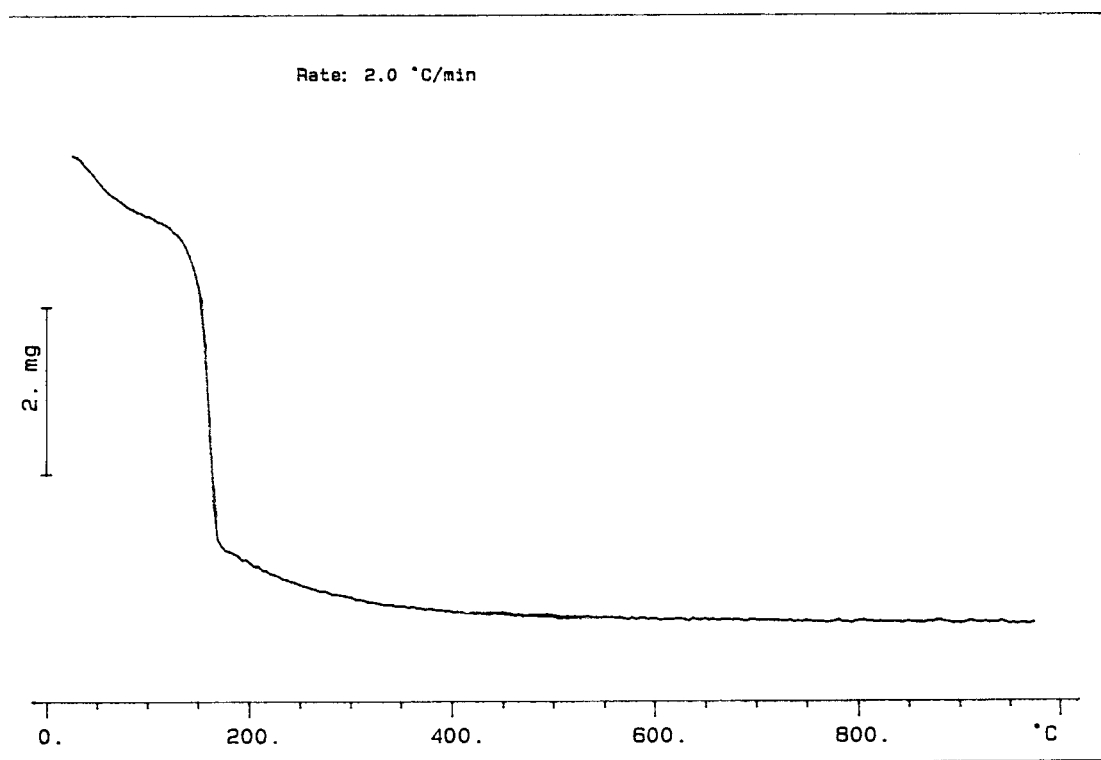


Figure 3.3. Thermogravimetric Analysis of Cu(OH)₂

3.2 Co₃O₄ NANOPARTICLES

a. Literature Review

Co₃O₄ nanoparticles have been synthesized through various chemical techniques. Aqueous cobalt (II) salt solutions have been heated in the presence of oxygen to obtain a

nanosized Co_3O_4 precipitate.⁷ They have been produced by solid-state oxidation of cobalt metal clusters dispersed in a polymeric matrix²⁶. Nanosized Co_3O_4 has also been produced from cobalt (II) acetate using a sonochemical method.¹⁹ In this work, $\text{Co}(\text{NO}_3)_2$, cobalt (II) nitrate, was reacted with NaOH to obtain $\text{Co}(\text{OH})_2$, cobalt (II) hydroxide, which upon annealing yielded Co_3O_4 particles as small as 9.4nm. This route to nanostructured Co_3O_4 was not found upon surveying the publications.

b. Synthesis

Preparation of $\text{Co}(\text{OH})_2$ Gel. $\text{Co}(\text{OH})_2$ gel was prepared in a manner similar to that of the $\text{Cu}(\text{OH})_2$ gel. 1M NaOH aqueous solution was added quickly to 0.1M $\text{Co}(\text{NO}_3)_2$ aqueous solution to a pH of 13 (i.e.p. of $\text{Co}(\text{OH})_2$ is 11.4)¹⁷ to obtain the greenish-blue precipitate $\text{Co}(\text{OH})_2(\text{H}_2\text{O})_4$.¹⁴ The chemical equation and reaction mechanism are analogous to that for $\text{Cu}(\text{OH})_2$ formation.¹⁴ The water-soluble species $\text{Co}(\text{OH})^{3-}(\text{H}_2\text{O})_3$ and $\text{Co}(\text{OH})^{4-}(\text{H}_2\text{O})_2$ are also present at pH=13.¹⁴ The resulting gel was isolated by filtration, washed with distilled water, dried at 50°C for 16 hours, then powdered.

Transformation of $\text{Co}(\text{OH})_2$ to Co_3O_4 . The $\text{Co}(\text{OH})_2$ powder was heated to form Co_3O_4 nanoparticles. CoO particles could not be obtained because of oxidation of cobalt during heating.

c. Characterization

Existence of pure Co_3O_4 was verified by XRD. Particle sizes of 9.4, 11.5, 10.4, 12.4, 17.0, 42.0, and 45.5nm were obtained from heating at 140, 150, 200, 300, 400, 800, and 950°C respectively (see figure 3.4). Co_3O_4 particle size was found to increase as annealing temperature was increased (see figure 3.5).

A 20.344mg sample of $\text{Co}(\text{OH})_2$ was analyzed using TGA (see figure 3.6). 0.9mg, or 4.424% of the sample weight, was lost in the form of adsorbed water over a temperature range of 25 to 130°C. When heated above 130°C, $\text{Co}(\text{OH})_2$ lost 2.725mg as it converted to Co_3O_4 . The percent weight loss in this phase transformation is

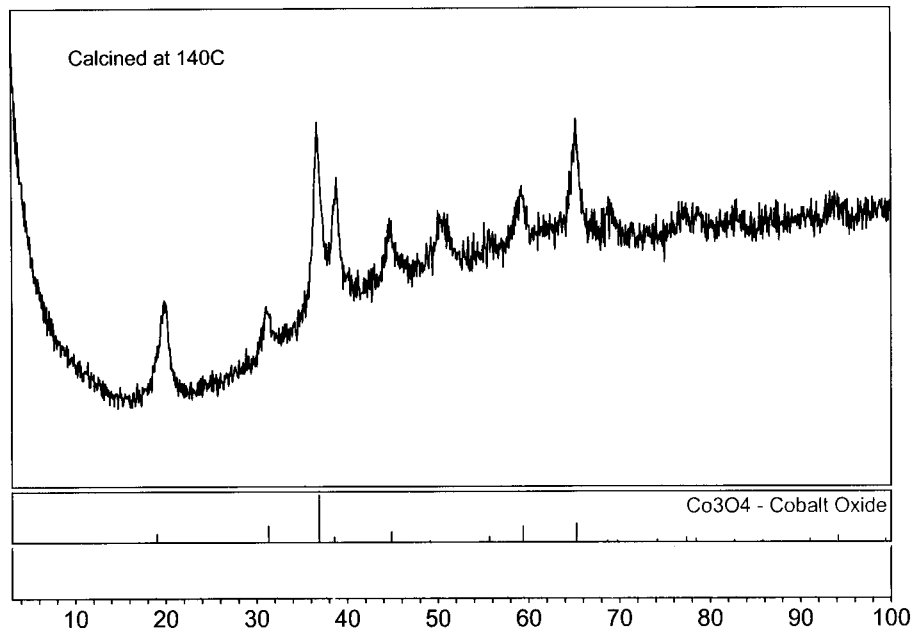


Figure 3.4. X-Ray Diffraction Pattern for Co_3O_4 (9.4nm particles)

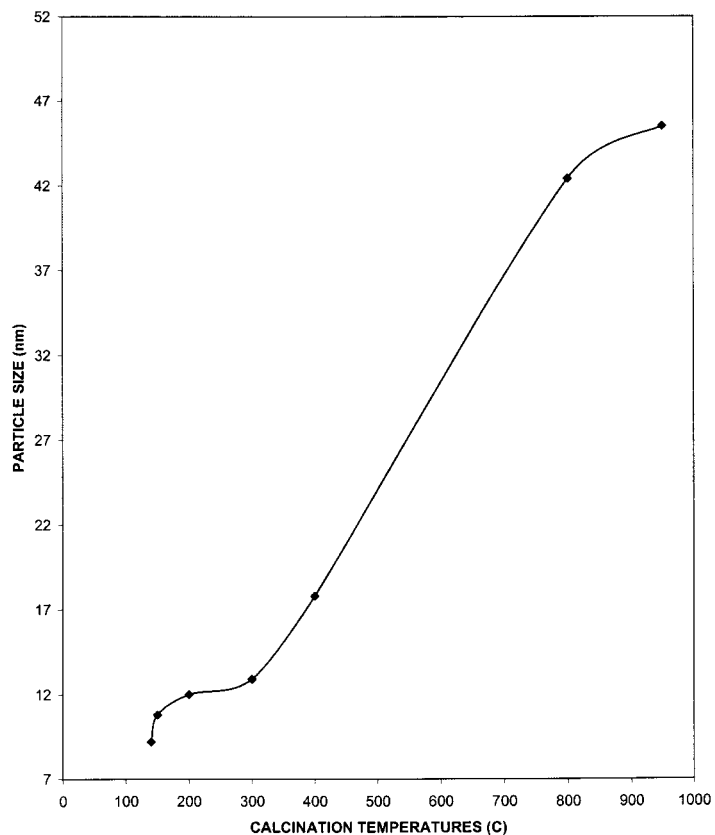


Figure 3.5. Co₃O₄ Particle Size vs. Annealing Temperature

$(2.725/19.444)*100\% = 14.0\%$, in close agreement with the theoretical value of 13.65%.

Three formula units of Co(OH)₂ lose two water molecules and two hydrogen atoms as it converts to Co₃O₄.



Therefore the theoretical weight loss of conversion is

$$\begin{aligned} & \{\text{Molecular weight of } (2\text{H}_2\text{O} + \text{H}_2)\} / \text{molecular weight of } 3\text{Co(OH)}_2 \} * 100\% \\ & = (38.06/3*92.95)*100\% = 13.65\% \end{aligned} \quad (3.8)$$

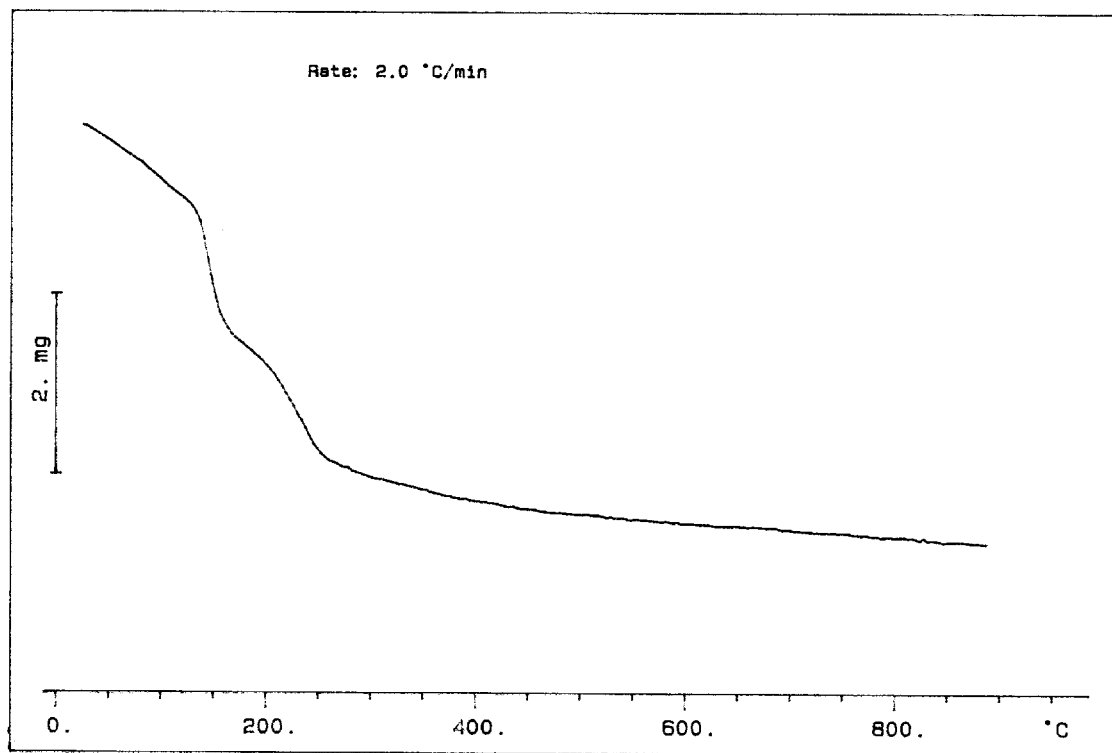


Figure 3.6. Thermogravimetric Analysis of $\text{Co}(\text{OH})_2$

3.3 Mn_5O_8 NANOPARTICLES

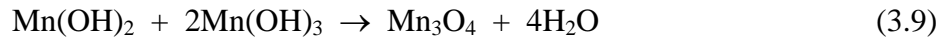
a. Literature Review

14-nm Mn_5O_8 was obtained by annealing Mn_3O_4 in air at 400°C for three hours. In surveying publications on Mn_5O_8 , heating Mn_3O_4 was the only preparation method found.^{27, 28, 29, 30} Our Mn_3O_4 sample was prepared from reaction of $\text{Mn}(\text{NO}_3)_2$, manganese nitrate, with NaOH . A literature search revealed that manganese salt reacted with base is the standard chemical preparation for Mn_3O_4 .³¹ Only one paper, published by Azzoni et al,²⁷ was found to explicitly state the particle size of their Mn_5O_8 sample

prepared, which was 21nm. Magnetic studies conducted on our 14-nm Mn₅O₈ samples were presented in a paper which has been submitted to *IEEE Transactions on Magnetics* for publication.

b. Synthesis

An initial attempt to produce MnO from annealing chemically-prepared Mn(OH)₂ failed. A stable sample of Mn(OH)₂ could not be prepared from reaction of Mn(NO₃)₂ and NaOH. Mn²⁺ partially oxidizes to Mn³⁺ giving Mn₃O₄, hausmannite.³¹



5g of Mn(NO₃)₂ were dissolved in 75mL of distilled water (0.1M). 125 mL of 1M NaOH were quickly added at room temperature to the nitrate solution. The pH of the solution was about 13, while the i.e.p is about 7.0.¹⁷ The brown precipitate, confirmed through XRD to be pure Mn₃O₄, was centrifuged and washed with water. Annealing at 200°C, the sample remained Mn₃O₄. Annealing the fresh Mn₃O₄ at 400°C gave Mn₅O₈. At temperatures of 600, 800, and 1000°C, Mn₂O₃ formed.

c. Characterization

XRD confirmed the formation of 14-nm pure Mn₅O₈ from annealing chemically prepared Mn₃O₄ at 400°C in air for three hours (see figure 3.7).

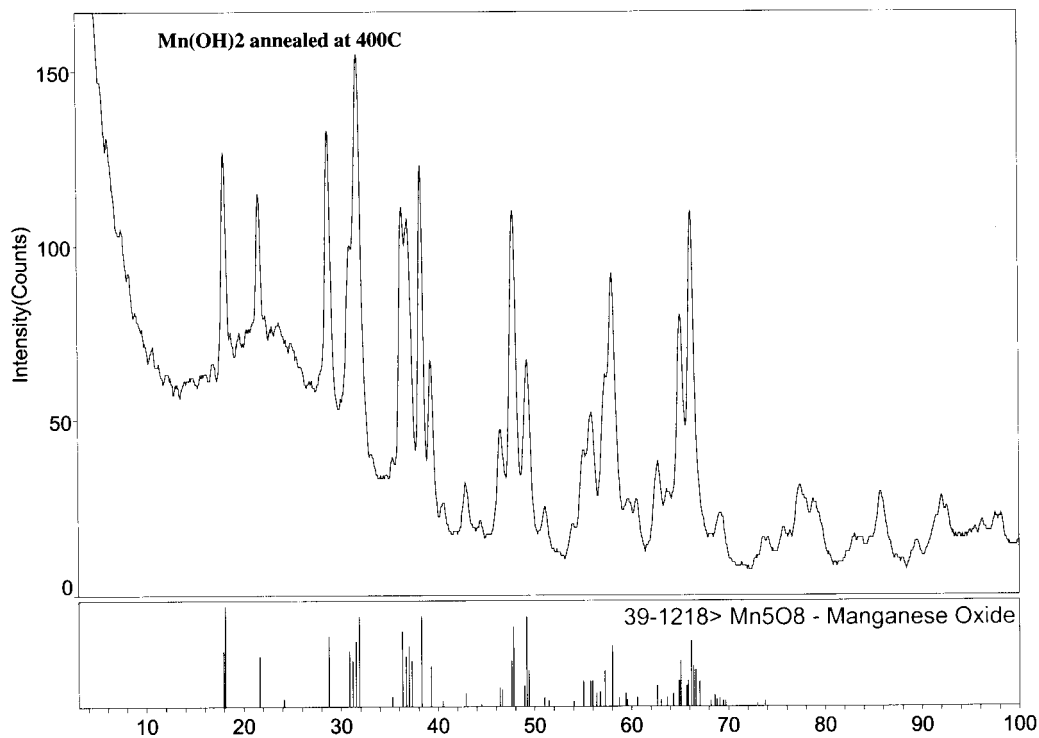


Figure 3.6. X-Ray Diffraction Pattern for Mn_5O_8

TGA revealed that Mn_3O_4 lost adsorbed water over a temperature range of 25 to 230°C (see figure 3.8). Mn_3O_4 gained oxygen from 230 to 400°C.



Above 400°C, Mn_5O_8 lost oxygen as it converted to Mn_2O_3 .



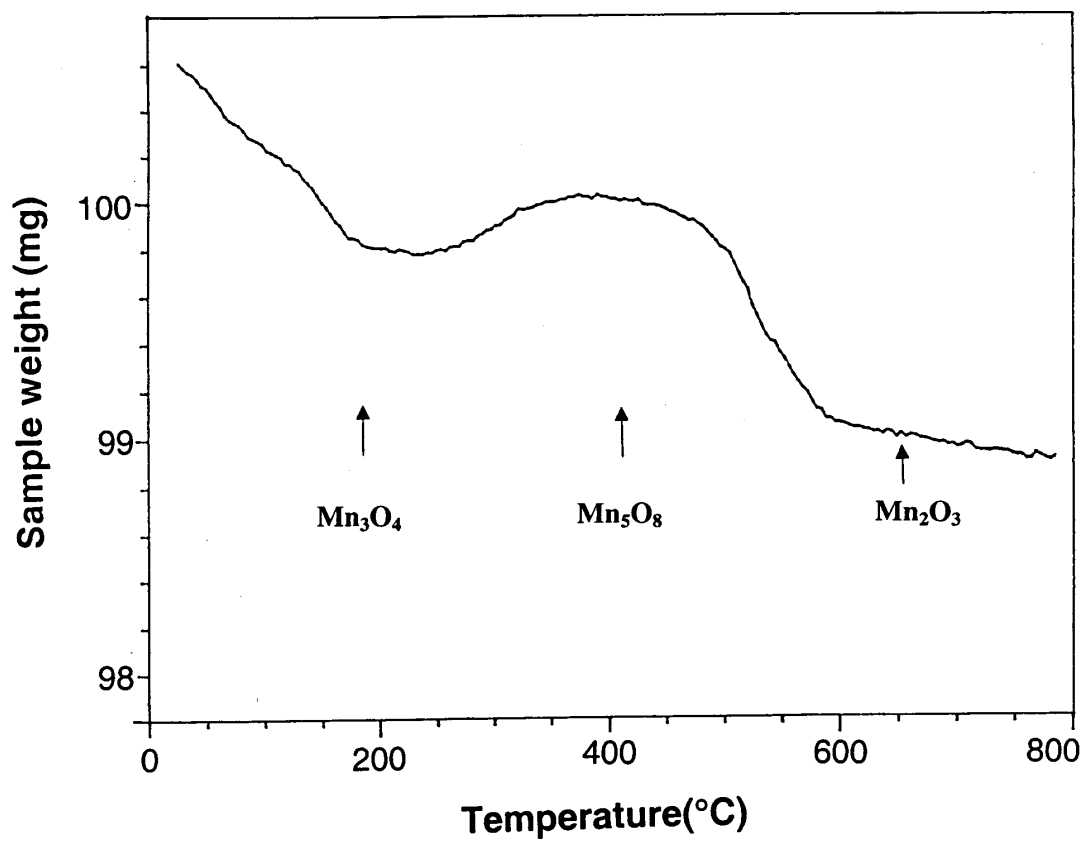


Figure 3.8. Thermogravimetric Analysis of Mn_3O_4

IV. FUNDAMENTALS OF ELECTROCHEMICAL SYNTHESIS

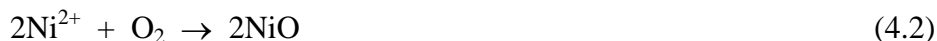
NiO nanoparticles were produced through an electrochemical route modeled after the procedures of Reetz et al². Reetz produced both Ni and Pd nanoclusters of dimensions between 2.2 and 4.8 nm.

An electrochemical cell was constructed using a nickel plate as anode and a platinum plate as cathode. The electrolytic solution consisted of the solvents acetonitrile (AN) and tetrahydrofuran (THF) in a 4:1 ratio with tetraoctylammonium bromide (TOAB) as the supporting electrolyte and stabilizer. In Reetz's experiment, TOAB effectively stabilized nickel nanoclusters. TOAB has also been shown to stabilize metal oxide nanoparticles,^{21,32} and so it seemed a good candidate as surfactant for the NiO nanoparticles in our experiment.

The nickel plate is a sacrificing anode, meaning that it donates the nickel atoms to be used in NiO synthesis. Upon applying a current density, creating an overpotential, Ni atoms at the anode are oxidized to Ni²⁺ cations, which tend to leave the bulk metal and enter the solution.



In Reetz's experiment, an argon atmosphere was used to prevent formation of NiO, while in our experiment, an oxygen atmosphere was used to encourage formation of NiO.



As NiO clusters form, TOAB adheres to particle surfaces giving a steric sol (see figure 4.1). The TOAB-stabilized NiO clusters are insoluble in the AN/THF solution making isolation of the particles possible through centrifugation.

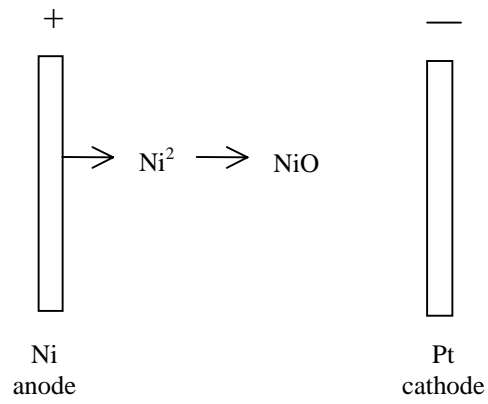


Figure 4.1. Electrochemical Production of NiO Nanoparticles

V. ELECTROCHEMICAL PREPARATION OF NiO NANOPARTICLES

a. Literature Review

CuO²¹ and ZnO³² nanoparticles have been prepared through electrochemical methods in the manner of Reetz et al.² However, electrochemical preparation of NiO nanoparticles was not found in the literature.

b. Synthesis

The electrolyte solution was prepared by dissolving TOAB in 200 mL of AN/THF (4:1) to a molarity of 0.1. The electrolyte, nickel anode, and platinum cathode system was isolated in a closed glass vessel with an oxygen atmosphere. The glass vessel was sealed with a rubber stopper, through which the electrode wires passed, and then placed in an ultrasonic bath to promote mixing. A current density of 0.1 mA/cm² was applied for three days over which time the solution turned from clear to cloudy-green. The green solid was separated by centrifugation and washed with THF/AN.

c. Characterization

XRD confirmed that the product formed was NiO with particle size 30nm (see figure 3.7). The broad background peaks are due to the TOAB coating on the particles.

VI. RESULTS AND CONCLUSIONS

CuO, Co₃O₄ and Mn₅O₈ nanoparticles were successfully synthesized from metal nitrate precursors using a sol-gel chemical route. Reaction of Cu(NO₃)₂ and NaOH aqueous solutions produced a Cu(OH)₂ gel, which upon annealing for three hours at

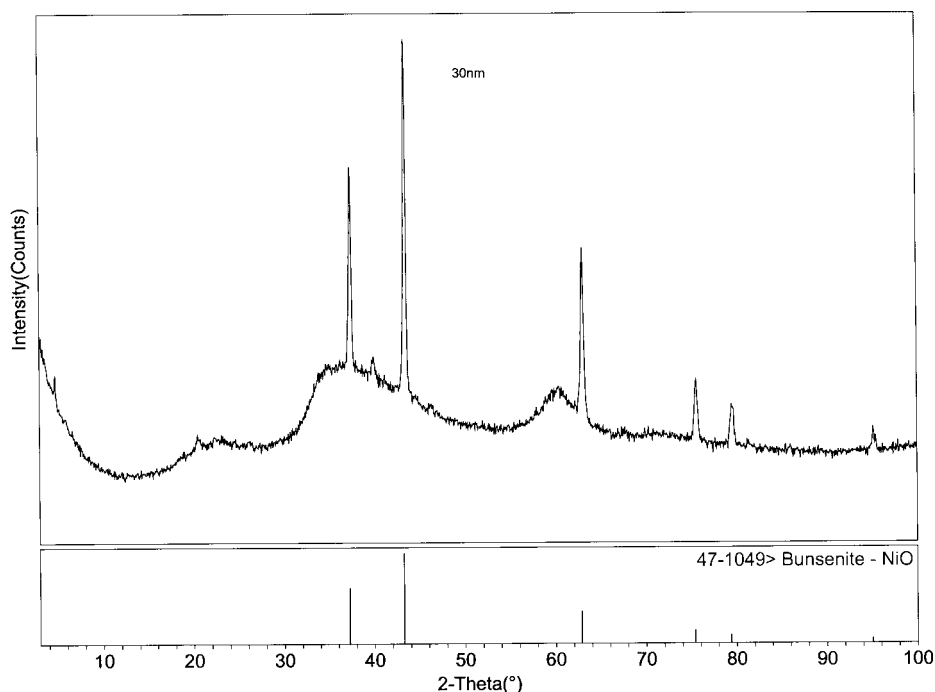


Figure 4.2. X-Ray Diffraction Pattern for NiO

temperatures of 160, 200, 250, 300, 400, 600, 800 and 1,000°C yielded CuO particles of 6.1, 7.8, 8.8, 11.6, 16.4, 25.7, 34.5 and 36.0nm respectively. These sizes are probably as small as can be expected from solution-chemistry preparation methods. Precipitated particles smaller than about 5nm are generally not obtainable because of their tendency to dissolve and reprecipitate onto surfaces of larger particles.

Co₃O₄ nanoparticles of sizes 9.1, 10.2, 12.1, 13.4, 17.0, 41.9, and 45.5nm were successfully prepared from heating a Co(OH)₂ gel, derived from Co(NO₃)₂ and NaOH, at temperatures of 140, 150, 200, 300, 400, 800 and 950°C respectively.

A pure 14nm-sample of the metastable Mn₅O₈ was prepared from annealing Mn₃O₄ for three hours at 400°C. Reaction of Mn(NO₃)₂ with NaOH gave the Mn₃O₄.

30-nm NiO particles were prepared from an electrochemical method using a nickel metal plate as a sacrificing anode. Generally, a much smaller particle size can be achieved from electrochemistry than from chemical precipitation. Metal oxide particles in a range of 1 to 4nm have been prepared electrochemically,^{21,32} so room for improvement in this NiO preparation method probably exists. Possibly, varying parameters such as current density, distance between electrodes, and surfactant concentrations could result in smaller particle sizes. The sample was washed with an acetonitrile/tetrahydrofuran solution which removed some of the surfactant tetraoctylammonium bromide. Maybe less washing, leaving a thicker coating, would better prevent coagulation resulting in smaller particle sizes.

REFERENCES

1. Nalwa, H.S., "Handbook of Nanostructured Materials and Nanotechnology," Vol. I. Synthesis and Processing, Academic Press, San Diego, CA, 2000, p. ix.
2. Reetz, M.T., and Helbig, W., *J. Am. Chem. Soc.*, **116**, pp. 7401-7402 (1994).
3. Sapijesko, R.S., and Matijevic, E., *Corrosion*, **36** (10), pp. 522-530 (1980).
4. Mazdiyasi, K.S., Lynch, C.T., and Smith, J.S., *J. Am. Ceram. Soc.*, **48** (7), pp. 372-375 (1965).
5. Pierre, A.C., "Introduction to Sol-Gel Processing," Kluwer Academic Publishers, Norwell, MA, 1998, pp. 2-17, 26, 27, 92-95, 140, 141, 182-185, 232-245, 278-287, 300-331.
6. Lee, S.H., Her, Y.S., and Matijevic, E., *J. Colloid Interface Sci.*, **186**, pp. 193-202 (1997).
7. Sugimoto, T., and Matijevic, E., *J. Inorg. Nuclear Chem.*, **41** (2), pp. 165-172 (1978).
8. Makhlof, S.A., Parker, F.T., Spada F.E., and Berkowitz, A.E., *J. Appl. Phys.*, **81** (8), pp. 5561-5563 (1997).
9. Matijevic, E., and Scheiner, P., *J. Colloid Interface Sci.*, **63** (3), pp. 509-524 (1977).
10. Sugimoto, T., and Matijevic, E., *J. Colloid Interface Sci.*, **74** (1), pp. 227-243 (1980).
11. Matijevic, E., Budnik, M., and Meites, L., *J. Colloid Interface Sci.*, **61** (2), pp. 302-311 (1977).

12. Blesa, M.A., Maroto, A.J.G., Passaggic, S.I., Figliolia, N.E., and Rigotti, G., *J. Mater. Sci.*, **20**, pp. 4601-4609 (1985).
13. Spanhel, L., and Anderson, M.A., *J. Am. Chem. Soc.*, **113**, pp. 2826-2833 (1991).
14. Baes, C.F., and Mesmer, R.E., "Hydrolysis of Cations," John Wiley & Sons, New York, N.Y., 1976, pp. 5, 219-226, 238-247, 267-275.
15. Vold, M.J., and Vold, R.D., "Colloid Chemistry: The Science of Large Molecules, Small Particles, and Surfaces," Reinhold Publishing Corp., New York, N.Y., 1964, pp. 1-36.
16. Brinker, C.J., and Scherer, G.W., "Sol-Gel Science: The Physics and Chemistry of Sol-Gel Processing," Academic Press, San Diego, CA, 1990, pp. 240, 244, 360, 362, 384, 402, 413, 414, 424, 444, 445, 453, 464, 501, 506, 562.
17. Parks, G.A., *Chem. Rev.*, **65**, pp. 177-198 (1965).
18. Hunter, R.J., "Zeta Potential in Colloid Science," Academic Press, New York, N.Y., 1981, pp. 228-229, 278-279.
19. Kumar, R.V., Diamant, Y., and Gedanken, A., *Chem. Mater.*, **12**, pp. 2301-2305 (2000).
20. Brookshier, M.A., Chusuei, C.C., and Goodman, D.W., *Langmuir*, **15** (6), pp. 2043-2046 (1999).
21. Borgohain, K., Singh, J.B., Rao, M.V.R., Shripathi, T., and Mahamuni, S., *Phys. Rev. B*, **61** (16), pp. 11 093-11 096 (2000).
22. Kratochvil, S., and Matijevic, E., *J. Mater. Res.*, **6** (6), pp. 766-777 (1991).
23. Ibrahim, M.M., Zhao, J., and Seehra, M.S., *J. Mater. Res.*, **7** (7), pp. 1856-1860 (1992).

24. Palker, V.R., Ayyub, P., Chattopadhyay, S., and Multani, M., *Phys. Rev. B*, **53** (5), pp. 2167-2170 (1996).
25. Ramamurthy, P., and Secco, E., *Can. J. Chem.*, **47**, pp. 3915-3918 (1969).
26. Verelst, M., Ely, T.O., Amiens, C., Snoeck, E., Lecante, P., Mosset, A., Respaud, M., Broto, J.M., and Chaudret, B., *Chem. Mater.*, **11**, pp. 2702-2708 (1999).
27. Azzoni, C.B., Mozzati, M.C., Galinetto, P., Paleari, A., Massarotti, V., Capsoni, D., and Bini, M., *Solid State Commun.*, **112**, pp. 375-378 (1999).
28. Wolska, E., and Kaczmarek, J., *Solid State Phenom.*, **39-40**, pp. 153-156 (1994).
29. Fritsch, S., Sarrias, J., Rousset, A., and Kulkarni, G.U., *Mater. Res. Bull.*, **33** (8), pp. 1185-1194 (1998).
30. Sugawara, M., Ohno, M., and Matsuki, K., *Chem. Lett.*, **8**, pp. 1465-1468 (1991).
31. Moon, J., Awano, M., Takagi, H., and Fujishiro, Y., *J. Mater. Res.*, **14** (12), pp. 4594-4601 (1999).
32. Mahamuni, S., Borgohain, K., and Bendre, B.S., *J. Appl. Phys.*, **85** (5), pp. 2861-2865 (1999).

VITA

Name: Heidi Jo Magnone

Parents: Gary B. Davenport
Donna S. Davenport

Husband: James J. Magnone, Jr.

Birthplace: Martin's Ferry, Ohio

Date of Birth: July 18, 1970

Schools Attended: St. Clairsville High School, St. Clairsville, OH 1984 – 1988
Ohio University Eastern, St. Clairsville, OH 1988 – 1990
Ohio University, Athens, OH 1990 – 1993
Wheeling Jesuit University, Wheeling, Wheeling, WV 1993 – 1995

Degrees Received: B.S., Physics, Wheeling Jesuit University 1995